

Impact of the Overall Electrical Filter Shaping in Next-Generation 25 and 50 Gb/s PONs

*Original*

Impact of the Overall Electrical Filter Shaping in Next-Generation 25 and 50 Gb/s PONs / TORRES FERRERA, Pablo; Ferrero, Valter; Valvo, Maurizio; Gaudino, Roberto. - In: JOURNAL OF OPTICAL COMMUNICATIONS AND NETWORKING. - ISSN 1943-0620. - STAMPA. - 10:5(2018), pp. 493-505. [10.1364/JOCN.10.000493]

*Availability:*

This version is available at: 11583/2704732 since: 2018-04-23T14:23:53Z

*Publisher:*

IEEE OSA

*Published*

DOI:10.1364/JOCN.10.000493

*Terms of use:*

This article is made available under terms and conditions as specified in the corresponding bibliographic description in the repository

*Publisher copyright*

IEEE postprint/Author's Accepted Manuscript

©2018 IEEE. Personal use of this material is permitted. Permission from IEEE must be obtained for all other uses, in any current or future media, including reprinting/republishing this material for advertising or promotional purposes, creating new collecting works, for resale or lists, or reuse of any copyrighted component of this work in other works.

(Article begins on next page)

# Impact of the Overall Electrical Filter Shaping in Next-Generation 25 and 50 Gb/s PONs

Pablo Torres-Ferrera, Valter Ferrero, Maurizio Valvo, and Roberto Gaudino

**Abstract**—Next-generation high-speed passive optical networks (HS-PONs) supporting 25, 50, and 100 Gb/s are in the early stages of their standardization process. One key aspect under discussion is the choice of the best modulation format for the transceivers. Performance comparisons among several modulation formats against different physical constraints have been presented in literature and are still being examined. In our present contribution, we performed an exhaustive analysis on the impact of the electrical frequency response of transceivers on the performance of two-level pulse amplitude modulation (PAM-2), 4-level PAM (PAM-4), electrical duobinary, and optical duobinary modulation formats with adaptive equalizers on the receiver side. We show, by means of numerical simulations, that the specification of the typically used  $-3$  dB bandwidth is insufficient, since out-of-band electrical frequency response specifications (such as the  $-20$  dB bandwidth) have a huge impact on the performance of the analyzed modulation formats. We believe that the normalized performance graphs given at the end of the paper in terms of  $-3$  dB and  $-20$  dB bandwidths can thus be useful for the design of next-generation HS-PON transceivers.

**Index Terms**—Adaptive equalization; APD; Duobinary; Filtering; PAM; PON.

## I. INTRODUCTION

Standardization efforts to define the physical layer characteristics of next-generation high-speed passive optical networks (HS-PONs) are currently being carried out in the International Telecommunication Union (ITU), Full Service Access Network (FSAN) Group, and the Institute of Electrical and Electronics Engineers (IEEE) standardization bodies [1–5]. Several research analyses are currently ongoing to choose the best modulation format for HS-PON transceivers for different bit rates under consideration (such as 25, 40, and 50 Gb/s) [6–17]. Due to a low cost constraint, particularly for the optical network unit (ONU) (i.e., user) side, several groups are considering if the transmitter and receiver optoelectronics developed for lower bit rates can be re-used for the new

higher capacity transceivers when associated to more bandwidth efficient modulation formats and/or adaptive equalization (AEQ). In particular, it would be interesting to re-use the optoelectronics developed for a 10 Gb/s PON for the 25 Gb/s target (and even for the 40 or 50 Gb/s ones), and similarly re-use the 25 Gb/s technology developed for the intra-datacenter short-range transceivers, also for 40–50 Gb/s PONs.

The motivation of this work is thus to analyze the feasibility of these goals, focusing on the fact that these transceivers would be severely electrically band-limited when used for the new target bit rates envisioned for HS-PONs (25 and 50 Gb/s). While previous papers in this area usually only focus on the  $-3$  dB bandwidth [18,19], or experimentally on a single given transceiver, we believe our approach is unique because this paper demonstrates, through extensive analyses, the strong impact of the overall frequency transfer function on system performance. We analyzed traditional intensity-modulation transmitters and direct-detection (DD) receivers followed by a digital signal processing (DSP)-based adaptive equalizer. We show that the *out-of-band* transceiver electrical frequency response is important for the modulation formats under consideration that are PAM-2 (i.e., binary on-off keying), PAM-4, electrical duobinary (EDB) [6,11], and optical duobinary (ODB) [8]. Specifically, we provide normalized graphs showing the joint impact of the  $-3$  dB and  $-20$  dB parameters of the frequency response on the system performance. We believe that these graphs offer a useful contribution to the current discussion in the aforementioned HS-PON standardization bodies and to the transceiver vendors that, depending on the details of their optoelectronic technology, can better select how to optimize their component design.

Thanks to our simulative approach, we were able to span a very large set of parameters ( $-3$  dB bandwidth,  $-20$  dB bandwidth, accumulated dispersion, etc.) and then obtain power penalty curves at a specific bit error rate (BER) value for the four different modulation formats. Moreover, we superimposed on our simulative results the expected bandwidths of several existing transmitters and receivers, thus giving a very broad review of the existing literature in this field.

Summarizing our previous considerations, we believe that the main contribution of this paper is in offering design rules for the transceivers' full electrical frequency

Manuscript received February 2, 2018; revised March 6, 2018; accepted March 6, 2018; published 0, 0000 (Doc. ID 321310).

P. Torres-Ferrera (e-mail: pablo.torres@polito.it), V. Ferrero, and R. Gaudino are with Politecnico di Torino, Dipartimento di Elettronica e Telecomunicazioni, Torino, Italy.

M. Valvo is with Telecom Italia (TIM), Torino, Italy.

<https://doi.org/10.1364/JOCN.99.099999>

response for different modulation formats. Consequently, our analysis points out the different resiliencies of each modulation format to variations in the available bandwidth and provides information that again can be interesting for component designers. We also report an extensive review of the transfer function of many transmit and receive options (TXs and RXs) presented in the literature, and we give their positioning in our performance estimation graphs.

To this end, the paper is organized in six sections. In Section II, we present the details of the considered transceiver and link architecture and of our simulation environments. In Section III, we discuss different frequency response characteristics, and apply it in Section IV, evaluating the resulting power budget penalty versus filter shape parameters. In Section V, we also introduce the impact of the typical chromatic dispersion accumulated in a PON for different choices of the wavelength band. Finally, we draw a conclusion in Section VI.

## II. SIMULATION SETUP

The transceiver and link architecture that we considered in our simulation setup is shown in Fig. 1, where the variable optical attenuator (VOA) is used to span different values of link loss, including the impact of the  $1 \times N$  PON splitting ratio. For space limitation, we will not consider the penalty arising from burst mode transmission. Apart from this (important [20]) consideration, our analysis can be applied to both the downstream and upstream directions of a PON link.

At the transmitter side, a binary signal at bit rate  $R_b$  (equal to either 25 or 50 Gb/s) is generated by means of a pseudorandom bit sequence (PRBS)  $2^{17} - 1$  bits long. The bit stream feeds the electrical TX that creates the appropriate driving signal to generate PAM-2, PAM-4, EDB, or ODB signals in the optical domain. We considered the use of external modulation in this paper or more in general optical transmitters characterized by negligible chirp. The generated electrical signal indicated as  $x(t)$  in Fig. 1 is obtained in different ways depending on the modulation format:

(i) In PAM-2 and PAM-4 cases, the binary signal is mapped into a 2-level or 4-level symbol stream, respectively. Gray coding is used in PAM-4.

(ii) In both EDB and ODB cases, the binary signal is digitally pre-coded by applying a standard XOR-based scheme [11]. The resulting 2-level pre-coded signal will eventually turn into a 3-level DB signal thanks to the intrinsic low-pass filtering response of the transceiver. We avoid the use of additional add-and-delay encoding or low-pass electrical filter circuits.

Time-domain simulations are performed using internally developed code fully written in a well-known commercial numerical software. Eight samples per bit (spb) were set. The signal  $x(t)$  is normalized to  $0 \leq x(t) \leq 1$ . We then assume that the DSP can compensate the Mach-Zehnder modulator (MZM)  $\cos^2(\cdot)$  instantaneous nonlinear response by applying the pre-distortion,

$$x_D(t) = \frac{A}{\pi} \arccos(1 - 2x(t)) - V_b, \quad (1)$$

where  $A$  is an amplitude factor and  $V_b$  is the bias-voltage of the MZM. The pre-distorted signal  $x_D(t)$  is then filtered using an electrical low-pass filter (LPF) that emulates the electrical frequency response of the TX. The shape of this filter (and the following one at the RX) is one of the main goals of our investigation. Details on the assumed filter shapes will be given in the Section III. The resulting electrical signal after filtering,  $x_F(t)$ , drives an optical modulator, optically fed by a continuous wave (CW) electrical field,  $E_{CW}(t)$ , generated by the TX laser. The electrical LPF, the optical modulator, and the laser compose the externally modulated laser (EML) block. The optical signal at the output of the EML is modeled using a classical (chirpless) MZM equation,

$$E_{EML}(t) = E_{CW}(t) \cos \frac{\pi x_F(t)}{V_\pi}, \quad (2)$$

where  $V_\pi$  is the  $\pi$ -voltage of the modulator. By setting both parameters,  $A$  and  $V_b$ , of Eq. (1) equal to  $V_\pi/2$  for PAM-2, PAM-4, and EDB, or equal to  $V_\pi$  for ODB, the MZM is operated in quadrature or null, respectively. The modulated optical signal is then propagated through a conventional single-mode fiber (SMF). Only chromatic dispersion is considered in the fiber model since the nonlinear effects are assumed to be negligible for the relatively short reach ( $\leq 20$  km) applications and power levels under study. The received optical signal is detected by means of an avalanche photodetector (APD) at the receiver (RX) side followed by a transimpedance amplifier (TIA). The APD + TIA configuration currently seems to be the most likely to be applied for a 40-gigabit-capable PON (NG-PON2) and a 10-gigabit-capable symmetric PON (XGS-PON), which is why we decided to focus on it. The photocurrent that outputs the APD + TIA is evaluated by

$$i(t) = \text{GRP}(t) + n_S(t) + n_T(t), \quad (3)$$

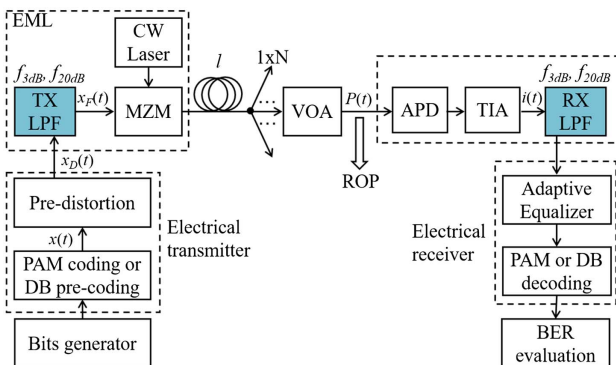


Fig. 1. Simulation setup.

178 where  $R$  is the APD responsivity (assumed to be  
179  $R = 0.8$  A/W),  $G$  is the APD gain factor [assumed to be  $G =$   
180  $25$  (14 dB)] [21,22], and  $P(t)$  is the optical signal instantane-  
181 ous power that feeds the APD. The signals  $n_S(t)$  and  
182  $n_T(t)$  emulate the shot noise and thermal noise, respec-  
183 tively. They are modeled as Gaussian random processes  
184 with zero-mean and variances given by [23]

$$\sigma_S^2(t) = qG^2FRP(t)\Delta f_s, \quad (4)$$

$$\sigma_T^2 = N_0\Delta f_s, \quad (5)$$

185 respectively, where  $F$  is the APD excess noise factor (we as-  
186 sume  $F = G^{0.75} = 10.5$  dB),  $q$  is the electron charge,  $N_0$  is  
187 the input-referred electrical current thermal noise power  
188 spectral density ( $N_0 = 1.024 \times 10^{-21} \text{A}^2/\text{Hz}$ ), and  $\Delta f_s$  is  
189 the bandwidth of the simulation ( $\Delta f_s = \text{spb} \cdot R_b$ ). The over-  
190 all thermal noise of APD and TIA contributions are in-  
191 cluded in the  $n_T(t)$  noise term. The numerical values  
192 assumed here are just indicative values for today's typical  
193 10G PON receivers. Since we present our results in terms  
194 of the relative power penalty among different modulation  
195 formats (see Sections IV and V), their actual values, how-  
196 ever, will have relatively little impact on the penalty  
197 graphs.

198 After the APD + TIA, an electrical LPF emulates the RX  
199 frequency response. The characteristics of this RX LPF are  
200 the same as the TX LPF, and they are described in the next  
201 section. We know that this is not the more general case  
202 since the TX and RX filter shapes are independent. We in-  
203 troduce this assumption to limit the number of free param-  
204 eters to be spanned. In the next section, an extended  
205 discussion regarding this consideration is presented.

206 Since we want to focus on severely band-limited trans-  
207 ceivers, we assume that the received electrical signal is  
208 equalized by an adaptive feed-forward equalizer (FFE) us-  
209 ing least-mean square (LMS) as an adaptation algorithm  
210 [19,24] with two samples per symbol and 20 taps. This  
211 number of taps was selected to guarantee the right opera-  
212 tion of the system in very dispersive and band-limited  
213 scenarios. In some cases, however, the system can operate  
214 with fewer taps without an additional penalty. The equal-  
215 izer is trained with a proper pilot sequence, which for  
216 PAM-2, PAM-4, and ODB is simply the original transmit-  
217 ted symbol sequence. For EDB, we use a 3-level DB symbol  
218 stream obtained after encoding the input pre-coded signal  
219 by means of an add-and-delay block. The equalized signal  
220 is then decoded according to the employed modulation for-  
221 mat. Finally, the bit error rate (BER) is evaluated using di-  
222 rect error counting over  $1.3 \times 10^5$  bits (after the training  
223 sequence), a situation that is very CPU-time demanding,  
224 but allows very precise estimation of the BER around  
225 the  $10^{-3}$  target value.

226 The main figure of merit employed in this work to evalu-  
227 ate the performance of the system is the sensitivity (S),  
228 defined as the received optical power (ROP) in dBm to  
229 reach a BER target of  $10^{-3}$  (i.e., the pre-FEC value selected,  
230 for instance, for NG-PON2 in ITU-T G.989.2 for 10 Gb/s).

### III. FILTERING CONSIDERATIONS

231

232 We emulate narrowband transceivers using two  
233 electrical LPFs, one at the TX side and one at the RX side.  
234 One key parameter of a transceiver frequency response is  
235 obviously its  $-3$  dB electrical bandwidth ( $f_{3\text{dB}}$ ). Most of the  
236 experimental and commercial device characterizations pro-  
237 vide information about this parameter. However, as the  
238 main target of our work, we focus on the fact that not only  
239 the  $f_{3\text{dB}}$  parameter is fundamental, but the out-of-band (i.  
240 e.,  $f > f_{3\text{dB}}$ ) frequency response of the devices also has a  
241 strong impact on the overall system performance. We show,  
242 for instance, that for the same  $f_{3\text{dB}}$  value, very different  
243 performance can be achieved depending on the actual value  
244 of, say, the  $-20$  dB bandwidth. Moreover, we will show that  
245 the sensitivity versus this last parameter is very different,  
246 depending on the modulation format used. To the best of  
247 our knowledge, this is a novel analysis for the HS-PON  
248 scenario, since the out-of-band transceiver electrical fre-  
249 quency characterization is barely ever considered in detail  
250 in the available literature. To investigate the relevance of  
251 this out-of-band filter shaping, we introduce the  $-20$  dB  
252 bandwidth parameter ( $f_{20\text{dB}}$ ) in our present analysis.  
253 The joint impact of the  $f_{3\text{dB}}$  and the  $f_{20\text{dB}}$  parameters is  
254 then tested, providing an extra degree of information re-  
255 garding the impact of the filtering shape on the perfor-  
256 mance. We present most of our results using the  
257 parameters  $B_{3\text{dB}}$  and  $B_{20\text{dB}}$ , which are a representation  
258 of  $f_{3\text{dB}}$  and  $f_{20\text{dB}}$ , respectively, normalized to the bit rate,  
259 expressed in percentages, and thus defined as

$$B_{3\text{dB}}[\%] = \frac{f_{3\text{dB}}}{R_b} \times 100 \quad \text{and} \quad B_{20\text{dB}}[\%] = \frac{f_{20\text{dB}}}{R_b} \times 100. \quad (6)$$

260 The degrees of freedom in electrical filter shapes are ob-  
261 viously infinite, so we had to make a somewhat arbitrary  
262 decision and select a few canonical transfer functions used  
263 in the literature [25]. We opted for the Butterworth (BF)  
264 and super-Gaussian filter (GF) profiles. Because the former  
265 is straightforward, it was selected to exactly set the desired  
266  $f_{3\text{dB}}$  parameter and to characterize it in terms of the num-  
267 ber of poles [25]. Moreover, the BF frequency response is as  
268 flat as possible in the passband [25], thus reducing, as com-  
269 pared to other filter types, the in-band shape variations (for  
270 a fixed passband bandwidth) when changing the out-of-  
271 band steepness. This feature is useful if researchers want  
272 to analyze the impact of the out-of-band shape variations  
273 as independently as possible on the in-band shape changes  
274 (as in the present contribution). However, in BF and for a  
275 fixed  $f_{3\text{dB}}$ , the value of the  $f_{20\text{dB}}$  parameter is subject to the  
276 choice of the number of poles of the filter (that is, an integer  
277 number) and, consequently,  $f_{20\text{dB}}$  can be only changed  
278 over given (and quite coarse) discrete values. Therefore,  
279 for BF, it is not possible to set any arbitrary combination  
280 of the  $f_{3\text{dB}}$  and  $f_{20\text{dB}}$  parameters. The use of GFs overcomes  
281 this limitation by allowing an independent variation of  
282  $f_{3\text{dB}}$  and  $f_{20\text{dB}}$ . The frequency profile of a GF is defined here  
283 as [26]

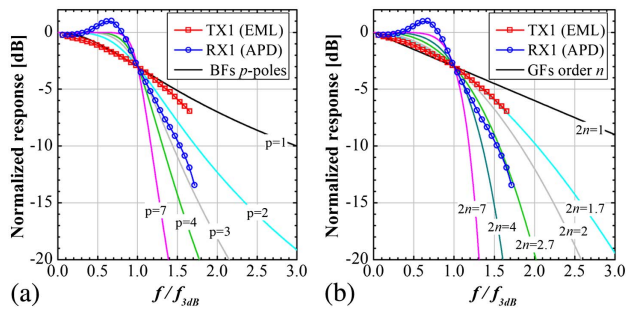


Fig. 2. (a) Butterworth (BF) and (b) Super-Gaussian filter (GF) profiles, for different numbers of poles and order, respectively. The normalized experimental response of the TX (EML) and the RX (APD) found in literature [17] are also shown.

$$H(f) = \exp\left(-\frac{1}{2}\left(\frac{f}{f_0}\right)^{2n}\right), \quad (7)$$

where  $n$  is the order of the GF filter (which now does not necessarily need to be an integer) and  $f_0$  is a free parameter. The two free and real values,  $n$  and  $f_0$ , can be set to obtain a frequency response having any possible combination of  $f_{3\text{dB}}$  and  $f_{20\text{dB}}$  (as long as  $f_{20\text{dB}} \geq f_{3\text{dB}}$ ). In Figs. 2(a) and 2(b), the filter shape profiles of the BF and GF models, respectively, are presented for different numbers of poles and order, using on the  $x$ -axis as the frequency normalized to  $f_{3\text{dB}}$ . The frequency responses of a realistic TX-RX pair experimentally reported in [17] are also displayed in the figure. From Fig. 2 it can be seen that, after a proper fitting of its two degrees of freedom, the GF model allows a good emulation of the out-of-band frequency response of the realistic TX and RX. The fitting using the BF model is less precise, due to the aforementioned discretization on the number of poles. This result also shows that a realistic transceiver cannot be easily modeled using zeros and poles rationale transfer functions if one must emulate accurately the frequency response also above the 3 dB band. Having said this, most of the results in Sections IV and V will be presented for both GF and BF models to have a full view of the filter shaping problem.

The most significant simplifying assumption made in this work is that the TX and RX LPFs are identical (i.e., they have the same filter shape). Although, this approach may not appear very realistic, a systematic analysis testing different combinations of  $f_{3\text{dB}}$  and  $f_{20\text{dB}}$  values in both the TX and RX filters would require studying a huge number of cases and several degrees of freedom, which is very impractical. We found that the equivalent filter formed after cascading any pair of TX and RX identical LPFs can approach well the overall equivalent frequency response formed by any particular combination of real TX and RX devices with different filter shaping (i.e., TX and RX with different  $f_{3\text{dB}}$  and  $f_{20\text{dB}}$  values). As a practical example, the same TX-RX pair taken from [17] and already represented in Fig. 2 (TX1 EML  $f_{3\text{dB}} = 8.9$  GHz, RX1 APD  $f_{3\text{dB}} = 7.5$  GHz) is used again in Fig. 3 to obtain the concatenated TX + RX transfer function, shown by a solid black curve. On the same figure, the response of the cascade of two identical GFs (or BFs) is shown in dashed green (or dotted pink, for a pair of

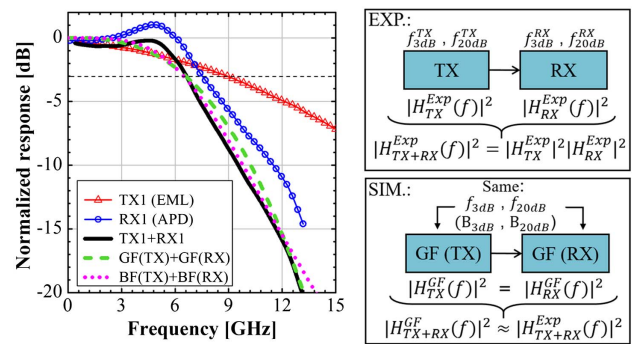


Fig. 3. Left side: TX (EML) and RX (APD) frequency characterization reported in [17]. In solid black, the TX+RX equivalent response. In dashed (dotted), the equivalent frequency response of a pair of identical GFs (BFs), with the same  $B_{3\text{dB}}$  and  $B_{20\text{dB}}$ . Right side: Diagram of our employed best-fitting procedure (EXP, Experimental data, and SIM, Simulation approach).

identical BFs) curve. In the case of GFs, a good matching with the solid black curve was obtained with two identical GFs, each with  $f_{3\text{dB}}$  equal to 8.5 GHz and  $f_{20\text{dB}}$  equal to 17 GHz. The equivalent pair of identical BFs are 2-pole filters, each with  $f_{3\text{dB}}$  equal to 8.1 GHz.

We followed this fitting procedure (shown in Fig. 3) for a large set of experimental devices reported in the literature. In particular, we evaluated the  $f_{3\text{dB}}$  and  $f_{20\text{dB}}$  values (and corresponding  $B_{3\text{dB}}$  and  $B_{20\text{dB}}$ ) of the GFs whose cascaded responses best matched the cascaded response of experimental or commercial TX + RX devices (see Fig. 3, right-hand diagram), and we summarized the results in Table I. Please note that all of these TX and RX devices were developed for standard NRZ 10 Gb/s transmission, which we will label in the rest of the paper as 10G

TABLE I  
NORMALIZED (FOR 25 OR 50 Gb/s TRANSMISSION) -3 dB AND -20 dB BANDWIDTH ( $B_{3\text{dB}}$  AND  $B_{20\text{dB}}$ ) FOR EACH OF THE IDENTICAL GFs AT TX AND RX WHOSE CASCADE RESPONSE BEST FITS THE EQUIVALENT RESPONSE OF THE TX + RX 10G COMPONENTS REPORTED IN THE REFERENCES

C.	TX (Exp.)		RX (Exp.)		GF, $R_b = 25$		GF, $R_b = 50$		T1:1 T1:2 T1:3 T1:4 T1:5 T1:6 T1:7 T1:8 T1:9 T1:10 T1:11 T1:12 T1:13 T1:14 T1:15
	Ref.	$f_{3\text{dB}}^{\text{TX}}$	Ref.	$f_{3\text{dB}}^{\text{RX}}$	$B_{3\text{dB}}$	$B_{20\text{dB}}$	$B_{3\text{dB}}$	$B_{20\text{dB}}$	
1	[17]	8.9	[17]	7.5	34	68	17	34	T1:3
2	[17]	8.9	[28]	8.8	32.8	112	16.4	56	T1:4
3	[17]	8.9	[29]	8.1	32	136	16	68	T1:5
4	[17]	8.9	[22]	6.8	29.6	96	14.8	48	T1:6
5	[27]	7.7	[17]	7.5	32	56	16	28	T1:7
6	[27]	7.7	[28]	8.8	27.6	80	13.8	40	T1:8
7	[27]	7.7	[29]	8.1	28	96	14	48	T1:9
8	[27]	7.7	[22]	6.8	26.8	72	13.4	36	T1:10
9	<sup>a</sup>	9.9	[17]	7.5	34	70	17	35	T1:11
10	<sup>a</sup>	9.9	[28]	8.8	35.2	100	17.6	50	T1:12
11	<sup>a</sup>	9.9	[29]	8.1	34.8	128	17.4	64	T1:13
12	<sup>a</sup>	9.9	[22]	7.5	31.6	92	15.8	46	T1:14
13	[30] <sup>b</sup>	$f_{3\text{dB}}^{\text{Sys}} = 6.3$ GHz			33.2	70	16.6	35	T1:15

C.: Case.  $f_{3\text{dB}}^{\text{TX}}$  and  $f_{3\text{dB}}^{\text{RX}}$  in GHz.  $B_{3\text{dB}}$  and  $B_{20\text{dB}}$  in %.  $R_b$  in Gb/s.  
<sup>a</sup>NG-PON2 TX characterization provided by Telecom Italia.  
<sup>b</sup>In this particular case,  $f_{3\text{dB}}^{\text{Sys}}$  indicates:  $f_{3\text{dB}}$  of the overall system.

TABLE II  
NORMALIZED (FOR 50 Gb/s TRANSMISSION)  $-3$  dB AND  $-20$  dB BANDWIDTH ( $B_{3\text{dB}}$  AND  $B_{20\text{dB}}$ ) OF EACH OF THE IDENTICAL GF'S AT TX AND RX WHOSE CASCADE RESPONSE BEST FITS THE EQUIVALENT RESPONSE OF THE TX + RX 25G COMPONENTS REPORTED IN THE REFERENCES

	TX (Exp.)			RX (Exp.)		GF, $R_b = 50$ Gb/s	
	C.	Ref.	[GHz]	Ref.	$f_{3\text{dB}}^{\text{RX}}$ [GHz]	$B_{3\text{dB}}\%$	$B_{20\text{dB}}\%$
T2:1							
T2:2							
T2:3	1	[31]	18.9	[33]	15.8	34	60
T2:4	2	[31]	18.9	[34]	24.5	40	132
T2:5	3	[31]	18.9	[35]	32	45	140
T2:6	4	[31]	18.9	[36]	19.9	40	88
T2:7	5	[32]	28.2	[33]	15.8	32	58
T2:8	6	[32]	28.2	[34]	24.5	50	130
T2:9	7	[32]	28.2	[35]	32	50	110
T2:10	8	[32]	28.2	[36]	19.9	44	88
T2:11	9	[27]	23.9	[33]	15.8	30	58
T2:12	10	[27]	23.9	[34]	24.5	42	84
T2:13	11	[27]	23.9	[35]	32	44	90
T2:14	12	[27]	23.9	[36]	19.9	38	78

technology. In Table II, the same information is reported for another set of experimental devices reported in literature for the 25 Gb/s transmission, called in this paper 25G technology. The information provided in Tables I and II is very helpful to contextualize our results in the framework of state-of-the-art technology.

From Table I, we can observe that the same couple of TX-RX devices has associated with a different pair of  $B_{3\text{dB}}$  and  $B_{20\text{dB}}$ , depending on the value of  $R_b$ . This arises because, although the  $f_{3\text{dB}}$  and  $f_{20\text{dB}}$  parameters of the corresponding identical GFs are the same irrespective of  $R_b$ , the  $B_{3\text{dB}}$  and  $B_{20\text{dB}}$  values are normalized to the bit rate, as indicated in Eq. (6).

#### IV. BACK-TO-BACK RESULTS

A back-to-back (BtB) performance comparison among the four modulation formats is presented in this section. For BtB, we mean a simulation that emulates the transceiver bandwidth limitations (thus taking into account only the filtering effects in the TX and RX), the electro-optical and opto-electrical conversions, and the noise at the receiver. The effect of the fiber (i.e., chromatic dispersion) will then be introduced in the next section.

We started the BtB analysis by considering 1-pole BF's as the electrical frequency response of each TX and RX device. In the inset of Fig. 4(a), we report the filter profiles of the individual TX, or RX, 1-pole BF (solid) and the cascaded response of them (dotted), for a (single filter)  $f_{3\text{dB}} = 7$  GHz. To enable a fair comparison, the performance is evaluated in terms of the power penalty taking as a reference the sensitivity of PAM-2 in its optimal conditions (without any BW limitations and in a BtB scenario). This sensitivity (the ROP to guarantee  $10^{-3}$  BER) is termed  $S_0$ , and, for the APD noise levels reported in the previous section, it is equal to  $S_0 = -28.1$  dBm for  $R_b = 25$  Gb/s, and  $S_0 = -25.7$  dBm for  $R_b = 50$  Gb/s. The computed power penalty

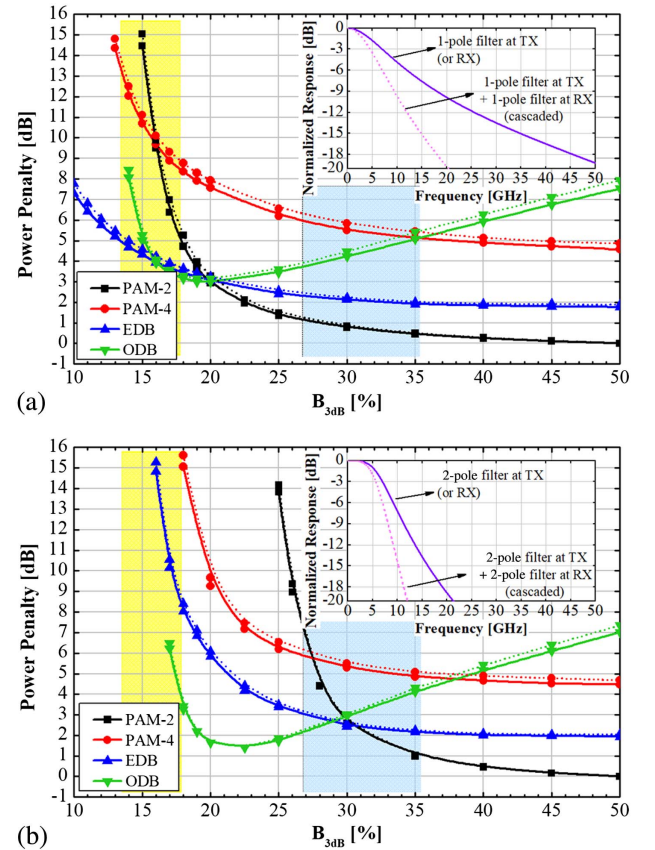


Fig. 4. Performance comparison among modulation formats in terms of the power penalty with respect to  $S_0$ , the PAM-2 sensitivity in the best condition (BtB unlimited bandwidth case,  $S_0 = -28.1$  dBm for 25 Gb/s and  $S_0 = -25.7$  dBm for 50 Gb/s), as a function of the  $B_{3\text{dB}}$  of the filters. (a) 1-pole BF and (b) 2-pole BF (depicted in the inset). Solid lines for  $R_b = 25$  Gb/s, dotted lines for  $R_b = 50$  Gb/s. Colored regions: In blue (yellow): 10G technology to transmit 25 (50) Gb/s.

of each modulation format as a function of the  $B_{3\text{dB}}$  parameter is shown in Fig. 4(a), for both analyzed bit rates: 25 Gb/s (solid) and 50 Gb/s (dotted). Thanks to the employed definition of the power penalty, there is a very close match between the results of the two analyzed bit rates, as demonstrated by the fact that the difference between the solid (25 Gb/s) and dotted (50 Gb/s) curves is negligible irrespective of the modulation format. By using the information provided in Table I, we also superimposed on Fig. 4 a pair of colored regions that qualitatively indicate the range of  $B_{3\text{dB}}$  values that current 10G transceivers exhibit when transmitting at 25 Gb/s (in blue) and 50 Gb/s (in yellow).

From Fig. 4 we can observe that in spite of using AEQ, the impact of limited system bandwidths is not completely canceled (as expected for an FFE-LMS-based AEQ [24] operating over a noisy signal). However, we have verified that the penalty due to system bandwidth reduction is much less pronounced using the AEQ scenario considered in this paper than for a not-equalized receiver (we cannot show the relative comparison here due to space limitations).

As discussed in the previous section, a 1-pole filter is very likely too optimistic for most realistic transceivers. To explore the impact of the out-of-band filter shaping on the analyzed modulation formats performance, the procedure to obtain the results presented in Fig. 4(a) is performed again using 2-pole BFs, but keeping the other assumptions the same. The corresponding results obtained under this new situation are presented in Fig. 4(b). One of the key points of our paper can be seen here: The out-of-band steepness of the transceivers' frequency response significantly affects the system performance even for the same  $-3$  dB bandwidth, and changes the performance ranking of the different modulation formats. For instance, let us consider the transmission of 25 Gb/s using 10G technology-based transceivers (case referred here as 25G/10G, shown in the blue-colored area of Fig. 4). In this situation, if the transceiver response is modeled using a 1-pole BF approach, PAM-2 outperforms the rest of the modulation formats in the complete 25G/10G (blue) region. However, if the filter's response model changes from one- to two-pole BF [Fig. 4(b)] PAM-2 starts to become critical, and it is, for instance, surpassed by EDB in part of the 25G/10G region of the graph. As another example, let us now consider the transmission of 50 Gb/s using 10G technology (case referred to here as 50G/10G, shown in the yellow colored area of Fig. 4). From Fig. 4(a), we can observe that EDB, ODB, and even PAM-4 (with a strong penalty) could be feasible alternatives for the 50G/10G transmission if a 1-pole filter case is considered (while PAM-2 is clearly out of the question). If we again change the filter response to a 2-pole profile, we can see from Fig. 4(b) that even EDB, ODB, or PAM-4 would operate in a region with exceedingly high penalty.

These first two examples show the performance dependency of the modulation formats versus the transceivers' frequency response, not only in terms of the  $-3$  dB bandwidth (as commonly done in much of the analysis in the current literature), but also as a function of the out-of-band (i.e., above the  $-3$  dB point) filter steepness.

We thus prosecute our analysis by also considering a parameter that would characterize the out-of-band response. As mentioned in Section III, we selected for this goal the frequency at a  $-20$  dB attenuation (i.e., the  $f_{20\text{dB}}$  parameter and its normalized version,  $B_{20\text{dB}}$ ). Note that another reference attenuation value could also have been chosen to quantify the degree of tilting of the out-of-band response. The use of the  $-20$  dB attenuation value was selected arbitrarily but, as we will show, it turned out to be a very relevant parameter.

To start the out-of-band filter impact analysis, we fixed the  $B_{3\text{dB}}$  parameter to 28%, which is a representative state-of-the-art case for the 25G/10G transmission as shown in Table I, and varied the number of poles of the BFs. As shown in Fig. 2(a), for a BF with a given  $f_{3\text{dB}}$ , increasing the number of poles corresponds to an increase in the out-of-band filter steepness, and a decrease in its  $-20$  dB bandwidth. The performance of the four modulation formats in terms of the relative power penalty as a function of the BF number of poles (or the corresponding  $B_{20\text{dB}}$  parameter) is shown in Fig. 5 (markers only), for 25 Gb/s transmission.

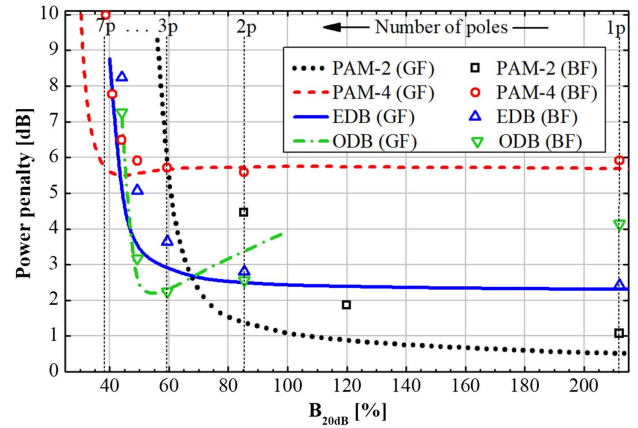


Fig. 5. Performance comparison in terms of  $B_{20\text{dB}}$  using BF (only marker curves) and GF (only line curves). A 25 Gb/s transmission is considered. The  $B_{3\text{dB}}$  is fixed to 28% ( $f_{3\text{dB}} = 7$  GHz for  $R_b = 25$  Gb/s). The power penalty is relative to PAM-2  $S_0 = -28.1$  dBm for  $R_b = 25$  Gb/s.

Since the number of poles is an integer parameter, only certain discrete  $B_{20\text{dB}}$  values can be evaluated. To overcome this too coarse discretization of  $B_{20\text{dB}}$ , the use of the GF model to emulate the transceiver frequency response is introduced. Under this GF approach, continuous curves of a relative power penalty versus  $B_{20\text{dB}}$  can now be obtained, and are depicted in Fig. 5 (curves without markers). Apart from the differences that occur using the BF or GF model, Fig. 5 shows with evidence the great relevance of the exact value of the out-of-band filter shape and, again, the fact that the performance ranking among modulation formats is also greatly affected by this parameter. For instance, although PAM-2 is the best modulation format in the  $B_{20\text{dB}} > 120\%$  region, for  $B_{20\text{dB}} \leq 70\%$  PAM-2 starts to become exceedingly critical in terms of the penalty. The EDB solution has, on the contrary, a good resilience for low  $B_{20\text{dB}}$  values, showing just small penalties down to the  $B_{20\text{dB}} = 50\%$  region. PAM-4 also exhibits a good tolerance, even for  $B_{20\text{dB}} = 40\%$ . ODB has a very peculiar behavior, showing both in Fig. 4 (versus  $B_{3\text{dB}}$ ) and Fig. 5 (versus  $B_{20\text{dB}}$ ) that it may be considered the best modulation format for very low bandwidths, but only if the  $B_{3\text{dB}}$  and  $B_{20\text{dB}}$  are optimized to their proper values. However, for  $B_{20\text{dB}} > 60\%$  values, the ODB sensitivity starts to get worse. The increased penalty shown with the GF approach is attributed to the reduced in-band power that this filter collects with respect to BFs for higher values of  $B_{20\text{dB}}$  (see Fig. 2). In the case of PAM-2, a close match between the BF and GF filter shape is only found when the filter steepness is very low (around the 1-pole BF case). Please note that for PAM-2, a point between the 1- and 2-pole cases was plotted. This point was measured by setting a 1-pole filter at the TX and a 2-pole filter at the RX (which corresponds to a 3-pole filter when the TX and RX filters are cascaded, emulating symmetric 1.5-poles at the TX and RX situation). This is the only exceptional point that was evaluated using different characteristics at TX and RX filters in this contribution. However, following the same approach, the performance of the system using a 1-pole filter at the TX and a 3-pole filter

F5:1  
F5:2  
F5:3  
F5:4  
F5:5

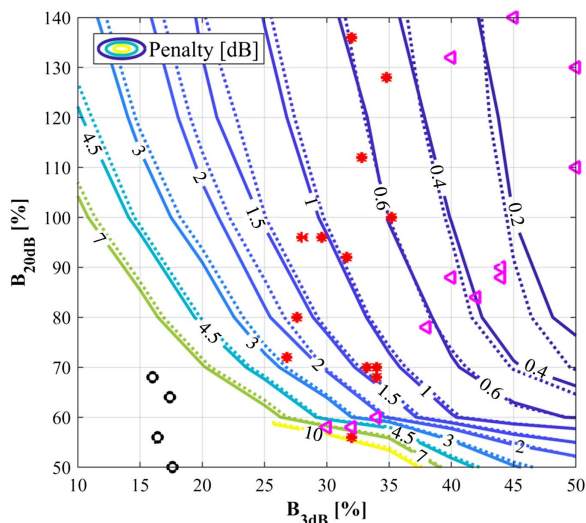
455  
456  
457  
458  
459  
460  
461  
462  
463  
464  
465  
466  
467  
468  
469  
470  
471  
472  
473  
474  
475  
476  
477  
478  
479  
480  
481  
482  
483  
484  
485  
486  
487  
488  
489  
490  
491  
492  
493

at the RX was also tested for PAM-2 (corresponding to a 4-pole filter when cascading the TX and RX, equivalent of having a 2-pole filter at the TX and one at the RX if a linear system is assumed). The sensitivity measured under this situation was the same as having 2-pole filters at TX and RX, which shows that the system behavior is mostly linear, and the cascaded assumptions described in Section III can be considered accurate.

To summarize, Fig. 5 suggests that when ranking the modulation format tolerance against the variation of the  $B_{20\text{dB}}$  parameter, PAM-4 and EDB show the best degree of resilience, PAM-4 being the most robust format for extremely low  $B_{20\text{dB}}$ , but obviously starting from its intrinsic penalty that is present compared to PAM-2 for high bandwidths. ODB has very interesting performance, but only for an optimized filter bandwidth, while EDB shows a very good compromise on a very large range of  $B_{20\text{dB}}$  values.

Compared to the actual data extrapolated from commercial transceivers and reported in the aforementioned Tables I and II, we can see that the  $B_{20\text{dB}}$  parameter can vary from around 60% to even 140%, for different state-of-the-art devices. This fact highlights the need to consider the robustness of a modulation format against both in-band and out-of-band filter shaping variations as a relevant parameter.

The results shown in Fig. 5 were obtained for a fixed value of  $B_{3\text{dB}} = 28\%$ . For different  $B_{3\text{dB}}$  values, the conclusions may change. We thus performed an extensive study on the impact of a joint variation of the  $B_{3\text{dB}}$  and  $B_{20\text{dB}}$  parameters. Results are presented in Fig. 6, which shows the power penalty of PAM-2 with respect to its best sensitivity  $S_0$  ( $S_0 = -28.1$  dBm for  $R_b = 25$  Gb/s, and



F6:1 Fig. 6. PAM-2 power penalty with respect to the S obtained for  
 F6:2 PAM-2 in the best condition (BtB unlimited bandwidth case,  $S_0 =$   
 F6:3  $-28.1$  dBm for 25 Gb/s and  $S_0 = -25.7$  dBm for 50 Gb/s) as a  
 F6:4 function of the GFs  $B_{3\text{dB}}$  and  $B_{20\text{dB}}$  parameters. Red points:  
 F6:5 25 Gb/s using 10G technology transceivers. Black circles:  
 F6:6 50 Gb/s using 10G technology transceivers. Pink triangles:  
 F6:7 50 Gb/s using 25G technology transceivers.

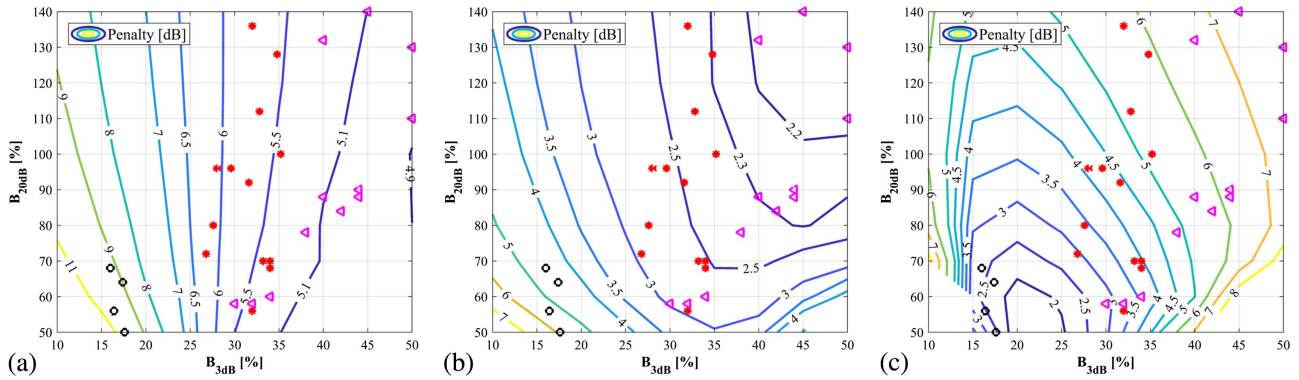
$S_0 = -25.6$  dBm for  $R_b = 50$  Gb/s) as a function of both  $B_{3\text{dB}}$  and  $B_{20\text{dB}}$  variables. We believe this is one of the key results of our paper, giving transceiver designers an overview of the best system solutions. Using this graph, a component designer can trade off the component parameters that most affect the  $B_{3\text{dB}}$  and  $B_{20\text{dB}}$ , and use the best design choices.

In Fig. 6, the contour plots in solid lines correspond to the 25 Gb/s case, while the ones in dotted lines to the 50 Gb/s transmission. A very good agreement between the solid and dotted curves is again found. Tables I and II show the real frequency response characteristics of the transceivers, which are also displayed in Fig. 6, in which any pair of  $B_{3\text{dB}}$  and  $B_{20\text{dB}}$  is considered as the coordinates of a point in the plane (indicating the operation regions of the current devices). Note the huge transceiver filter shaping impact on the performance. For instance, when using 25G transceivers for 50 Gb/s transmission (pink triangles), considering different real devices we can have a negligible penalty (lower than 0.2 dB in some cases), but in other cases the penalty can reach 10 dB. The same information is plotted in Fig. 7 for the other modulation formats, always evaluating the power penalty with respect to the same PAM-2  $S_0$  sensitivity values of Fig. 6. Since the same good agreement between the 25 and 50 Gb/s results found for PAM-2 was also corroborated for the other modulation formats, only 50 Gb/s curves (representing both bit rate situations) are shown.

By summarizing all the information provided by Figs. 4-7, we can state the following conclusions with respect to the filter shape impact on the performance of the four different modulation formats in the BtB situation. Let us start by considering the options to transmit 25 Gb/s using 10G technology transceivers (25G/10G):

- PAM-4 exhibits the best tolerance against filter shaping variations, in the sense that its penalty curve versus the reduction in filter bandwidth (for both  $B_{3\text{dB}}$  and  $B_{20\text{dB}}$ ) remains flat down to very low values. However, this format has a bigger penalty compared to EDB or ODB in the 25G/10G region [see the red points of Figs. 7(a)-7(c), and their associated power penalty].
- ODB exhibits large variations as a function of the  $B_{3\text{dB}}$  and  $B_{20\text{dB}}$  parameter. In the search for low transceiver bandwidth solutions, it has a very interesting behavior, but only around its optimal values. Moreover, it should be remembered that this is the only format that necessarily requires an external modulator (while all the other three modulation formats also can be implemented with directly modulated lasers).
- PAM-2 presents a strong filtering-dependent performance (see Fig. 6). For instance, by using two transceivers having the same  $B_{3\text{dB}} = 30\%$  but very different steepness (i.e.,  $B_{20\text{dB}} = 60\%$  and  $120\%$ , which is not far from a real situation, as shown by the red points in Fig. 6), a very different penalty of  $>7$  dB versus  $\sim 1$  dB, respectively, can be obtained. Therefore, PAM-2 is a good alternative only if large bandwidth transceivers are used.





F7:1 Fig. 7. (a) PAM-4, (b) EDB, and (c) ODB power penalty with respect to the S obtained for PAM-2 in the BtB unlimited bandwidth case,  $S_0$   
 F7:2 ( $S_0 = -28.1$  dBm for 25 Gb/s and  $S_0 = -25.7$  dBm for 50 Gb/s) as a function of  $B_{3dB}$  and  $B_{20dB}$  of the GFs. Red points: 25 Gb/s using 10G  
 F7:3 technology. Black circles: 50 Gb/s using 10G technology. Pink triangles: 50 Gb/s using 25G technology.

585 – EDB shows a good tolerance against filtering, and a penalty between 2 and 3 dB in all the cases reported in Table I.  
 586 Accordingly, EDB seems to be a very interesting alternative in terms of resilience against filtering variations (with  
 587 respect to both  $-3$  dB bandwidth and steepness).  
 588  
 589

590 Let us now consider the option of transmitting 50 Gb/s  
 591 using 10G technology (50G/10G):

592 – PAM-2 is not feasible (see the black circles of Fig. 6).  
 593 – Neither PAM-4 or EDB seem to be feasible alternatives,  
 594 since a large power penalty is achieved in this situation  
 595 [see the black circles of Figs. 7(a) and 7(b)].  
 596 – The only modulation format that may be used is ODB  
 597 [see the black circles of Fig. 7(c)]. However, in the  $B_{3dB} <$   
 598  $15\%$  range, the penalty of ODB rapidly increases even  
 599 with small  $-3$  dB bandwidth decreases. Therefore, the  
 600 performance stability can be critical.

601 Finally, let us consider transmitting 50 Gb/s using 25G  
 602 technology (50G/25G):

603 – For PAM-2 and EDB, the same conclusions as in the case  
 604 of 25G/10G can be extrapolated. However, most 25G tech-  
 605 nology has more relaxed bandwidth limitations to trans-  
 606 mit 50 Gb/s (see pink triangles in Fig. 6). PAM-2 then  
 607 seems to be a good alternative to transmit 50G/25G.  
 608 EDB only outperforms it if transceivers with very strong  
 609 bandwidth limitations are employed.  
 610 – PAM-4 and ODB are not good candidates since a large  
 611 power penalty ( $>3$  dB) arises in this situation.

## 612 V. DISPERSION ANALYSIS

613 In Section IV, the effect of the transceivers' filtering char-  
 614 acteristics on the performance of four IM/DD modulation  
 615 formats in a BtB scenario was analyzed. In this section,  
 616 the previous analysis is extended by also considering the  
 617 presence of chromatic dispersion in the link.

618 As a first approach, the  $B_{3dB}$  and  $B_{20dB}$  parameters are  
 619 fixed to some of the values discussed in the previous section

and the total dispersion of the link is varied to compute the  
 relative power penalty of the four modulation formats as a  
 function of this last parameter. For the 25 Gb/s transmis-  
 sion, two representative  $\{B_{3dB}, B_{20dB}\}$  pairs were selected:  
 $P1 = \{32\%, 136\%$  and  $P2 = \{32\%, 56\%$  (cases 5 and 3 of  
 Table I, respectively), to compare the power penalty versus  
 dispersion curves obtained when the  $-3$  dB bandwidth of the  
 filters is the same, but the steepness is abruptly  
 changed. The results are displayed in Fig. 8(a). For the  
 50 Gb/s situation, the following  $\{B_{3dB}, B_{20dB}\}$  pairs were  
 employed:  $P3 = \{32\%, 132\%$  and  $P4 = \{32\%, 58\%$  (case  
 5 of Table II). The corresponding results are shown in  
 Fig. 8(b).

From Fig. 8(a) ( $R_b = 25$  Gb/s), we can observe that  
 PAM-4 is the most robust format against the effect of both  
 dispersion and filtering. EDB also exhibits good tolerance  
 against dispersion. We now introduce some practical con-  
 sideration focusing on the PON scenario, which requires  
 using SMF fibers up to  $l = 20$  km in different wavelength  
 bands, which we have grouped as O-band (about 1300 nm,  
 where at the limit of the bandwidth specified by different  
 PON standards the accumulated dispersion can go  
 up to  $\sim 100$  ps/nm), C-band (1550 nm, accumulated  
 dispersion up to 360 ps/nm), and L-band (1580 nm, up  
 to  $\sim 460$  ps/nm). Comparing the different modulation

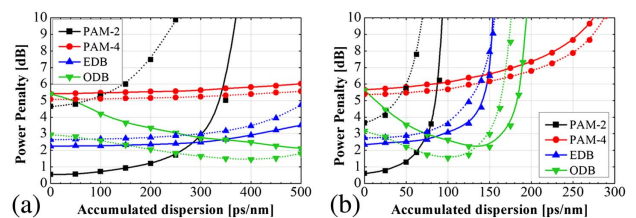


Fig. 8. Performance comparison among the four modulation  
 formats in terms of the relative power penalty as a function  
 of dispersion. (a)  $R_b = 25$  Gb/s; solid:  $B_{3dB} = 32\%$  and  $B_{20dB} =$   
 $136\%$ ; dotted:  $B_{3dB} = 32\%$  and  $B_{20dB} = 56\%$ ; (b)  $R_b = 50$  Gb/s;  
 solid:  $B_{3dB} = 32\%$  and  $B_{20dB} = 132\%$ ; dotted:  $B_{3dB} = 32\%$  and  
 $B_{20dB} = 58\%$ . The power penalty is relative to PAM-2  $S_0$   
 ( $S_0 = -28.1$  dBm for  $R_b = 25$  Gb/s and  $S_0 = -25.7$  dBm for  
 $R_b = 50$  Gb/s).

620  
 621  
 622  
 623  
 624  
 625  
 626  
 627  
 628  
 629  
 630  
 631  
 632  
 633  
 634  
 635  
 636  
 637  
 638  
 639  
 640  
 641  
 642  
 643  
 644  
 F8:1  
 F8:2  
 F8:3  
 F8:4  
 F8:5  
 F8:6  
 F8:7  
 F8:8

formats, EDB outperforms PAM-4 in O, C, and L optical bands. Regarding PAM-2, as in BtB, in presence of dispersion its performance is also highly affected by the steepness of the out-of-band transceivers' response. Its use in C- or L-band is not feasible for  $l = 20$  km. In O-band, its use seems to be strongly constrained to the use of technology with low steepness filtering characteristics. Under these conditions, its performance is the best among all modulation formats. ODB, on the other hand, is the only format in which the performance improves as both the dispersion and steepness of the filters increase (at least in O, C, and L bands with  $l = 20$  km). In O-band, ODB is outperformed by EDB, while in the C- and L-bands it seems to be the best alternative.

Regarding the 50 Gb/s transmission [see Fig. 8(b)] over 20 km of fiber, we observed that no modulation format can be used to operate the system in the C-band or L-band. PAM-2 does not work even in the O-band. The only feasible modulation formats (in O-band,  $l = 20$  km) are EDB, ODB, and PAM-4, being the performance of PAM-4 surpassed by that of both EDB and ODB in the whole O-band.

Although PAM-4 has been found to be the most resilient format against dispersion and bandwidth limitations in all the analyzed conditions, due to its higher intrinsic penalty as compared to EDB in all the practical scenarios, we do not consider it a feasible alternative for the implementation of 25 Gb/s or 50 Gb/s PON systems over 20 km of fiber. Therefore, we do not analyze this modulation format in the rest of this section. A similar consideration has been performed with respect to PAM-2 operating in the C-band with  $R_b = 25$  Gb/s, and the O-band with  $R_b = 50$  Gb/s. Therefore, other than the 25 Gb/s O-band case in which PAM-2 can still be considered a feasible format, the rest of this section will be focused on the comparison between EDB and ODB formats.

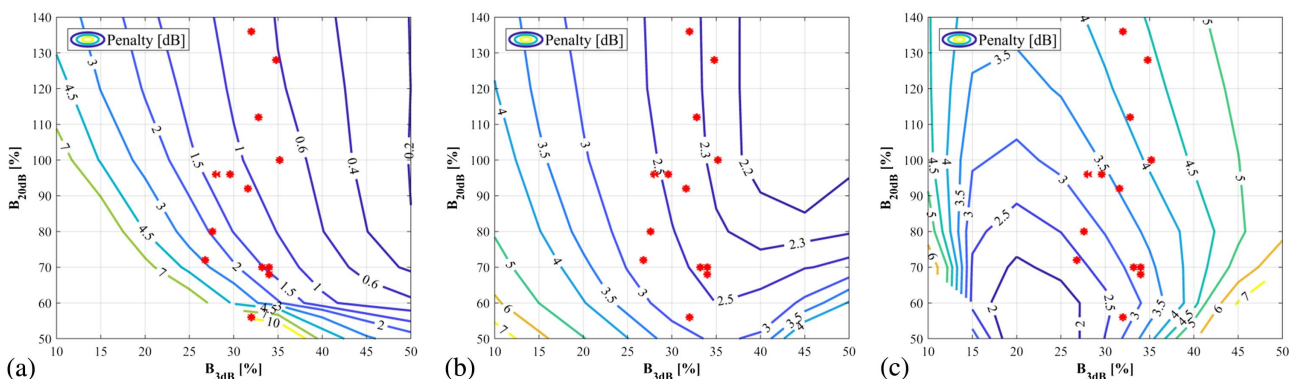
Some preliminary results allow us to forecast the feasibility of PAM-2 and PAM-4 using pre-chirping in the transmission of 50 Gb/s in the O-band and C-band ( $l = 20$  km), respectively, at least under relaxed bandwidth limitations (1-pole BF's case). However, these alternatives need to be further explored under more strict filtering

conditions, which is an analysis out of the scope of the present contribution.

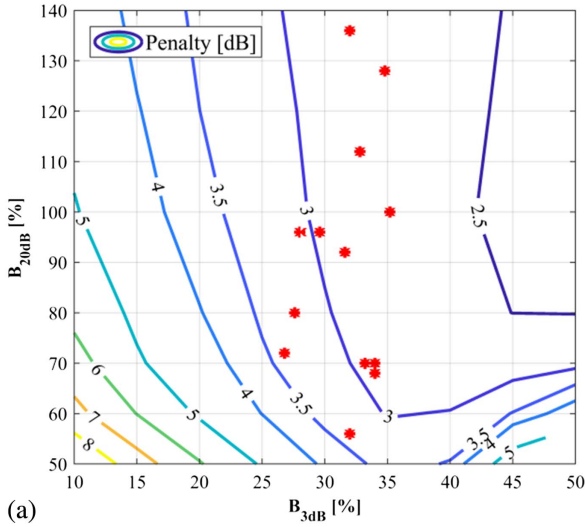
We now proceed with some further insight, focusing on 25 Gb/s transmission results. In Figs. 9 and 10 we show, for the O-band and the C-band operation over 20-km of fiber, respectively, the contour plots of the power penalty as a function of  $B_{3dB}$  and  $B_{20dB}$ , for different modulation formats and for different accumulated dispersion (using the previously indicated notation of the O- and the C-band at 20 km). The power penalty is evaluated in all cases with respect to  $S_0$  of PAM-2 in BtB conditions ( $S_0 = -28.1$  dBm for  $R_b = 25$  Gb/s).

Regarding O-band operation (Fig. 9), the three modulation formats exhibit similar results to the BtB situation (see Figs. 6 and 7), but have a small dispersion penalty for PAM-2 and EDB. In contrast, ODB exhibits a performance improvement thanks to dispersion, which is consistent with the results presented in Fig. 8. The power penalty of EDB varies between 2.2 and 3 dB when using state-of-the-art transceivers with different  $-3$  dB bandwidth and out-of-band filtering steepness. In contrast, in the case of PAM-2, this penalty can vary from around 0.6 to an exceedingly large value around 10 dB. ODB is an intermediate case (the penalty varies from 2.5 to 4.5 dB). Therefore, we consider EDB as the best alternative for 25 Gb/s 20-km O-band operation with respect to tolerance against frequency response variations. However, PAM-2 can be a good solution; its penalty can be as low as  $<1$  dB, which is a value not achievable by any other format, if *and only if* technology with proper filtering characteristics ( $B_{3dB} \geq 30\%$  and  $B_{20dB} \geq 70\%$ ) can be guaranteed.

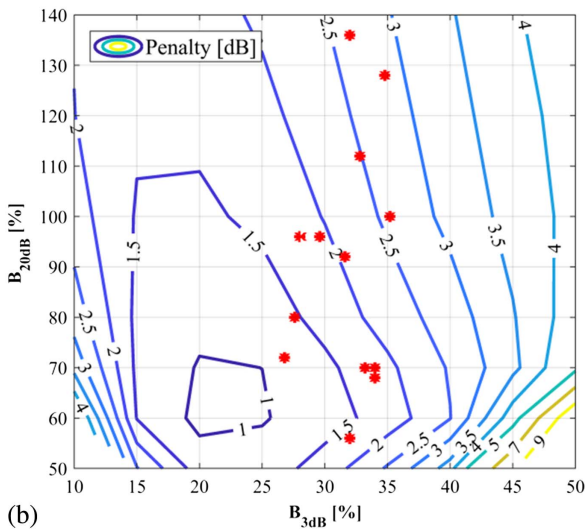
When considering C-band operation, we can see from the contour plots shown in Figs. 10(a) and 10(b), that the performance of ODB is further improved by dispersion while the opposite occurs for EDB. This situation tips the scales in favor of ODB in terms of a lower range of power penalty achievable using state-of-the-art devices (i.e., from 1 to 3 dB, in contrast to 2.5 to 3.5 dB achieved with EDB). EDB remains the format with less performance variations as a function of filtering. It is important to note that, by using ODB and small band-limited transceivers



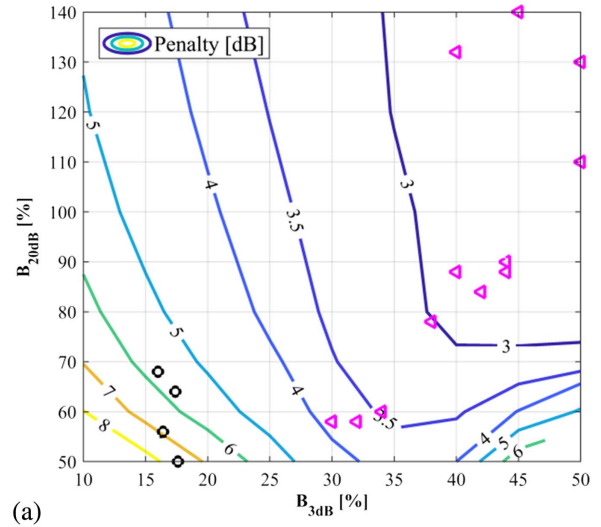
F9:1 Fig. 9. (a) PAM-2, (b) EDB, and (c) ODB power penalty with respect to the S obtained for PAM-2 in the BtB unlimited bandwidth case,  $S_0$   
F9:2 ( $S_0 = -28.1$  dBm) as a function of  $B_{3dB}$  and  $B_{20dB}$  of the GFs, for a 25 Gb/s/20 km O-band operation. Red points: 25 Gb/s using 10G  
F9:3 technology.



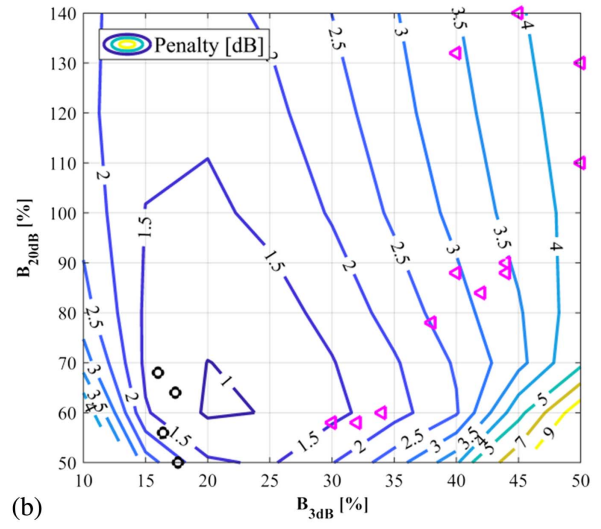
(a)



(b)



(a)



(b)

F10:1 Fig. 10. (a) EDB and (b) ODB power penalty with respect to the S  
 F10:2 obtained for PAM-2 in the BtB unlimited bandwidth case,  $S_0$   
 F10:3 ( $S_0 = -28.1$  dBm) as a function of  $B_{3dB}$  and  $B_{20dB}$  of the GFs,  
 F10:4 for a 25 Gb/s/20 km C-band operation. Red points: 25 Gb/s using  
 F10:5 10G technology.

F11:1 Fig. 11. (a) EDB and (b) ODB power penalty with respect to the S  
 F11:2 obtained for PAM-2 in the BtB unlimited bandwidth case,  $S_0$   
 F11:3 ( $S_0 = -25.6$  dBm) as a function of  $B_{3dB}$  and  $B_{20dB}$  of the GFs,  
 F11:4 for a 50 Gb/s 20 km O-band operation. Black circles: 50 Gb/s using  
 F11:5 10G technology. Pink triangles: 50 Gb/s using 25G technology.

(i.e.,  $B_{3dB} \geq 35\%$  and  $B_{20dB} \geq 100\%$ ), it is always possible to increase the performance of the system by intentionally adding an electrical filter at the TX or RX, to enforce a stronger band-limited condition [close to the optimum point that can be seen in Fig. 10(b)] in which the achievable penalty could be only 1 dB. This feature is not achievable using any other modulation format. Another positive (and unique) feature of ODB is that, as can be seen in Fig. 8, the dispersion penalty decreases as the accumulated dispersion increases (i.e., length), which can compensate, to some degree, for the increase of fiber attenuation as the fiber length augments. In favor of EDB is the fact that it can be implemented with both direct modulation and external modulation (using electro-absorption modulators or a MZM) approaches, while ODB must use a MZM.

Let us finally comment on the 50 Gb/s transmission results. In Fig. 11, contour plots of the power penalty as a

function of  $B_{3dB}$  and  $B_{20dB}$  for 50 Gb/s 20-km O-band operation using EDB [Fig. 11(a)] or ODB [Fig. 11(b)], are shown. The power penalty is referred to the 50 Gb/s PAM-2  $S_0 = -25.6$  dBm. The contour plots displayed in Fig. 11 are very similar to those shown in Fig. 10 (for 25 Gb/s transmission in 20-km O-band). However, the regions of operation of 50G/10G and 50G/25G state-of-the-art devices (see the black circles and pink triangles of Fig. 11, respectively) are different from those of 25G/10G (see the red points of Fig. 10). Therefore, the conclusions between these cases may differ. First, ODB appears to be the only feasible format to transmit 50 Gb/s using 10G technology in O-band. In the black circles of Fig. 11, only the cases 2, 3, 10, and 11 in Table I are plotted. The rest of the cases have a  $B_{20dB} < 50\%$ , which corresponds to power penalties higher than 2.5 dB [not shown in Fig. 11(b)]. Then, for

F11:1  
 F11:2  
 F11:3  
 F11:4  
 F11:5  
 744  
 745  
 746  
 747  
 748  
 749  
 750  
 751  
 752  
 753  
 754  
 755  
 756  
 757  
 758  
 759

correct operation, the  $B_{20\text{dB}}$  of the TX and RX should at least be higher than 50%.

Regarding the transmission of 50 Gb/s using 25G technology, the maximum penalty achievable with EDB [pink triangles in Fig. 11(a)] and ODB [pink triangles in Fig. 11(b)] is similar (around 4 dB). Again, EDB exhibits a more stable penalty, varying between 3 and 4 dB (mostly around 3 dB), while ODB penalty variation is wider, varying from 1.5 to 4 dB. In terms of tolerance against filtering, we should opt for EDB. However, as mentioned before, with the right technology characteristics or by enforcing the frequency response using an additional electrical filter, we could operate close to the optimal point of ODB and achieve a penalty as low as 1 dB.

## VI. CONCLUSIONS

In this contribution, we have demonstrated the strong impact on system performance that the overall filter shaping electrical response of the transceivers has on the transmission of 25 and 50 Gb/s using currently available 10 and 25 Gb/s technology and adaptive equalization. Using numerical simulations, we compared the achievable performance of PAM-2, PAM-4, EDB, and ODB under different band-limited and dispersive conditions. We introduced the  $-20$  dB bandwidth parameter to quantify the impact of the out-of-band steepness of the transceivers' response. We demonstrated that this parameter is as relevant as the  $-3$  dB bandwidth when comparing the performance of different modulation formats.

We found that PAM-2 is the best performing format for the transmission of 25 Gb/s using 10G technology in the 20 km O-band, but only if transceivers with relatively small bandwidth limitations can be used. Otherwise, the best alternative is EDB because it is more resilient to filter shaping variations than PAM-2 and outperforms the rest of the formats in terms of penalty.

On the transmission of 25 Gb/s using 10G technology in 20-km C-band, EDB exhibits a slightly higher maximum power penalty than ODB (4 dB versus 3.5 dB). The minimum achievable power penalty of ODB is 1.5 dB lower than that of EDB. However, the performance of EDB as a function of the  $-3$  dB and  $-20$  dB bandwidth is more stable (power penalty variations are less than 1 dB) than in the case of ODB, which has power penalty variations up to 2 dB.

Regarding the 50 Gb/s case, no modulation format works under 20 km of C-band operation. PAM-2 is not even feasible in the O-band. ODB is the only format that can be used if using 10G technology (in the 20 km O-band), but only if some filtering conditions can be guaranteed. If 25G technology is used and the O-band is considered through 20 km of fiber, both EDB and ODB can work, exhibiting a maximum penalty of 4 dB. Again, the penalty of ODB is the minimum under some filtering conditions, but EDB performance is more robust against the filter shaping variations of the transceivers' frequency response.

In all cases, PAM-4 is the most robust format against both dispersion and filtering conditions. However, due to its inherent higher power penalty with respect to the rest of the formats, PAM-4 is always outperformed by any of them in most of the analyzed conditions.

The results presented in this contribution were obtained using identical filters to emulate the frequency response of both the TX and RX. For space limitations, we did not consider more general assumptions and degrees of freedom in our present analysis. Using filters with different characteristics at the TX and RX side, which could give rise to interesting results, is a topic we are currently researching.

## ACKNOWLEDGMENT

This work was supported by Telecom Italia under the grant 5G-PON (2017). This work was carried out under the PhotoNext initiative at Politecnico di Torino (<http://www.photonext.polito.it/>).

## REFERENCES

- [1] IEEE P802.3ca 100G-EPON Task Force, "Physical layer specifications and management parameters for 25 Gb/s, 50 Gb/s, and 100 Gb/s passive optical networks," 2015 [Online]. Available: <http://www.ieee802.org/3/ca/index.shtml>.
- [2] Full Service Access Network (FSAN), "Roadmap," 2016 [Online]. Available: <https://www.fsan.org/roadmap/>.
- [3] ITU-T Study Group 15: Networks, "Technologies and infrastructures for transport, access and home," 2017 [Online]. Available: <https://www.itu.int/en/ITU-T/studygroups/2017-2020/15/Pages/default.aspx>.
- [4] V. Houtsma, D. van Veen, and E. Harstead, "Recent progress on standardization of next-generation 25, 50, and 100G EPON," *J. Lightwave Technol.*, vol. 35, no. 6, pp. 1228–1234, 2017.
- [5] D. Nasset, "PON roadmap [Invited]," *J. Opt. Commun. Netw.*, vol. 9, pp. A71–A76, 2017.
- [6] D. van Veen, V. E. Houtsma, P. Winzer, and P. Vetter, "26-Gbps PON transmission over 40-km using duobinary detection with a low cost 7-GHz APD-based receiver," in *European Conf. Optical Communication (ECOC)*, Amsterdam, The Netherlands, 2012.
- [7] Z. Li, L. Yi, X. Wang, and W. Hu, "28 Gb/s duobinary signal transmission over 40 km based on 10 GHz DML and PIN for 100 Gb/s PON," *Opt. Express*, vol. 23, pp. 20249–20256, 2015.
- [8] D. van Veen, V. Houtsma, A. H. Gnauck, and P. Iannone, "Demonstration of 40-Gb/s TDM-PON over 42-km with 31 dB optical power budget using an APD-based receiver," *J. Lightwave Technol.*, vol. 33, no. 8, pp. 1675–1680, 2015.
- [9] J. Wei, N. Eiselt, H. Griesser, K. Grobe, M. H. Eiselt, J. J. V. Olmos, I. T. Monroy, and J.-P. Elbers, "Demonstration of the first real-time end-to-end 40-Gb/s PAM-4 for next-generation access applications using 10-Gb/s transmitter," *J. Lightwave Technol.*, vol. 34, no. 7, pp. 1628–1635, 2016.
- [10] J. Man, S. Fu, H. Zhang, J. Gao, L. Zeng, and X. Liu, "Downstream transmission of pre-distorted 25-Gb/s faster-than-Nyquist PON with 10G-class optics achieving over 31 dB link budget without optical amplification," in *Optical Fiber Communication Conf. and Exhibition (OFC)*, Anaheim, California, 2016.

- 873 [11] D. van Veen and V. Houtsma, "Symmetrical 25-Gb/s TDM-  
874 PON with 31.5-dB optical power budget using only off-the-  
875 shelf 10-Gb/s optical components," *J. Lightwave Technol.*,  
876 vol. 34, no. 7, pp. 1636–1642, 2016.
- 877 [12] M. Tao, L. Zhou, S. Yao, D. Zou, S. Li, H. Lin, and X. Liu, "28-  
878 Gb/s/λ TDM-PON with narrow filter compensation and en-  
879 hanced FEC supporting 31.5 dB link loss budget after 20-  
880 km downstream transmission in the C-band," in *Optical  
881 Fiber Communication Conf. and Exhibition (OFC)*,  
882 Anaheim, California, 2016.
- 883 [13] V. Houtsma and D. van Veen, "A study of options for high-  
884 speed TDM-PON beyond 10G," *J. Lightwave Technol.*, vol. 35,  
885 no. 4, pp. 1059–1066, 2017.
- 886 [14] C. Sun, S. H. Bae, and H. Kim, "Transmission of 28-Gb/s  
887 duobinary and PAM-4 signals using DML for optical access  
888 network," *IEEE Photon. Technol. Lett.*, vol. 29, no. 1,  
889 pp. 130–133, 2017.
- 890 [15] D. van Veen and V. Houtsma, "Proposals for cost-effectively  
891 upgrading passive optical networks to a 25G line rate," *J.  
892 Lightwave Technol.*, vol. 35, no. 6, pp. 1180–1187, 2017.
- 893 [16] T. Minghui, L. Zhou, H. Zeng, S. Li, and X. Liu, "50-Gb/s/λ  
894 TDM-PON based on 10G DML and 10G APD supporting  
895 PR10 link loss budget after 20-km downstream transmission  
896 in the O-band," in *Optical Fiber Communication Conf. and  
897 Exhibition (OFC)*, Los Angeles, California, 2017.
- 898 [17] S. Yin, V. Houtsma, D. van Veen, and P. Vetter, "Optical am-  
899 plified 40-Gbps symmetrical TDM-PON using 10-Gbps optics  
900 and DSP," *J. Lightwave Technol.*, vol. 35, no. 4, pp. 1067–1074,  
901 2017.
- 902 [18] D. Liu and M. Tao, "50G single wavelength PON analysis and  
903 comparison," in *IEEE 802.3 NG-EPON Study Group Meeting*,  
904 Orlando, Florida, Nov. 2017 [Online]. Available: [http://www.  
905 ieee802.org/3/ca/public/meeting\\_archive/2017/11/liu\\_3ca\\_2a\\_  
906 1117.pdf](http://www.ieee802.org/3/ca/public/meeting_archive/2017/11/liu_3ca_2a_1117.pdf).
- 907 [19] A. Stark and T. Detwiler, "Equalization strategies for 25G  
908 PON," in *Optical Fiber Communication Conf. and  
909 Exhibition (OFC)*, Los Angeles, California, 2017.
- 910 [20] R. Bonk, W. Poehlmann, D. van Veen, J. Galario, R. Farah, H.  
911 Schmuck, and T. Pfeiffer, "The underestimated challenges of  
912 burst-mode WDM transmission in TWDM-PON," *Opt. Fiber  
913 Technol.*, vol. 26, pp. 59–70, 2015.
- 914 [21] J. Rue, M. Itzler, N. Agrawal, S. Bay, and W. Sherry, "High  
915 performance 10 Gb/s PIN and APD optical receivers," in  
916 *Electronic Components and Technology Conf.*, San Diego,  
917 California, 1999, pp. 207–215.
- 918 [22] N. Duan, T.-Y. Liow, A. E.-J. Lim, L. Ding, and G. Q. Lo, "310  
919 GHz gain-bandwidth product Ge/Si avalanche photodetector  
920 for 1550 nm light detection," *Opt. Express*, vol. 20, pp. 11031–  
921 11036, 2012.
- 922 [23] G. P. Agrawal, *Fiber-Optic Communication Systems*, 3rd ed.  
923 Wiley, 2002.
- 924 [24] J. G. Proakis, *Digital Communications*, 4th ed., McGraw-Hill,  
925 2000.
- 926 [25] J. G. Proakis and D. G. Manolakis, *Digital Signal Processing.  
927 Principles, Algorithms, and Applications*, 4th ed. Prentice  
928 Hall, 1996.
- 929 [26] S. Bottacchi, *Theory and Design of Terabit Optical Fiber  
930 Transmission Systems.*, Cambridge University, 2014.
- 931 [27] G. L. Li, T. G. B. Mason, and P. K. L. Yu, "Analysis of  
932 segmented traveling-wave optical modulators," *J.  
933 Lightwave Technol.*, vol. 22, no. 7, pp. 1789–1796, 2004.
- 934 [28] Spectrolab, "043643: 10 Gb/s InGaAs/InAlAs avalanche  
935 photodetector (APD) die," 2017 [Online]. Available:  
[http://www.spectrolab.com/sensors/pdfs/products/SR%20APD  
936 %2010G%20Die\\_RevA%20052512.pdf](http://www.spectrolab.com/sensors/pdfs/products/SR%20APD%2010G%20Die_RevA%20052512.pdf) 937
- [29] Y. Kang, M. Zadka, S. Litski, G. Sarid, M. Morse, M. J.  
938 Paniccia, Y.-H. Kuo, J. Bowers, A. Beling, H.-D. Liu, D. C.  
939 McIntosh, J. Campbell, and A. Pauchard, "Epitaxially-grown  
940 Ge/Si avalanche photodiodes for 1.3 μm light detection," *Opt.  
941 Express*, vol. 16, pp. 9365–9371, 2008. 942
- [30] F. Effenberger, "NRZ-NFC for 28G-PON," in *IEEE 802.3 NG-  
943 EPON Study Group Meeting*, Dallas, Texas, Nov. 2015  
944 [Online]. Available: [http://www.ieee802.org/3/NGEPONSG/  
945 public/2015\\_11/ngepon\\_1511\\_effenberger\\_3.pdf](http://www.ieee802.org/3/NGEPONSG/public/2015_11/ngepon_1511_effenberger_3.pdf) 946
- [31] M. Chagnon, M. Osman, M. Poulin, C. Latrasse, J.-F. Gagné,  
947 Y. Painchaud, C. Paquet, S. Lessard, and D. Plant,  
948 "Experimental study of 112 Gb/s short reach transmission  
949 employing PAM formats and SiP intensity modulator at  
950 1.3 μm," *Opt. Express*, vol. 22, pp. 21018–21036, 2014. 951
- [32] A. Samani, M. Chagnon, D. Patel, V. Veerasubramanian, S. 2  
952 Ghosh, M. Osman, Q. Zhong, and D. V. Plant, "A low-voltage  
953 35-GHz silicon photonic modulator-enabled 112-Gb/s trans-  
954 mission system," *IEEE Photon. J.*, vol. 7, no. 3, pp. 1–13, 2015. 3  
955
- [33] V. Houtsma, D. van Veen, A. Gnauck, and P. Iannone, "APD-  
956 based duobinary direct detection receivers for 40 Gbps TDM-  
957 PON," in *Optical Fiber Communications Conf. and Exhibition  
958 (OFC)*, Los Angeles, California, 2015. 959
- [34] Z. Huang, C. Li, D. Liang, K. Yu, C. Santori, M. Fiorentino, W.  
960 Sorin, S. Palermo, and R. G. Beausoleil, "25 Gbps low-voltage  
961 waveguide Si-Ge avalanche photodiode," *Optica*, vol. 3,  
962 pp. 793–798, 2016. 963
- [35] H. H. Lee, K.-H. Doo, S.-G. Mun, K. Kim, J. H. Lee, S.-K. Kang,  
964 H. Park, N. Park, H. Park, and H. S. Chung, "Real-time dem-  
965 onstration of QoS guaranteed 25-Gb/s PON prototype with  
966 Ethernet-PON MAC/PHY and cost-effective APD receivers  
967 for 100-Gb/s access networks," *Opt. Express*, vol. 24,  
968 pp. 13984–13991, 2016. 969
- [36] M. Nada, M. Nakamura, and H. Matsuzaki, "25-Gbit/s burst-  
970 mode optical receiver using high-speed avalanche photodiode  
971 for 100-Gbit/s optical packet switching," *Opt. Express*, vol. 22,  
972 pp. 443–449, 2014. 973  
974
- Pablo Torres-Ferrera** received B.E., M.E.E., and Ph.D. degrees  
975 (with honors) in Telecommunications in 2010, 2012, and 2017, re-  
976 spectively, from the National Autonomous University of Mexico  
977 (UNAM), Mexico City. He worked from 2012 to 2013 at Huawei  
978 Technologies Mexico in the implementation of OTN rings. As part  
979 of his Ph.D. investigation work, he carried out research internships  
980 at Athens Information Technology (AIT), Greece, in 2014 and at  
981 Politecnico di Torino, Italy, in 2016. He is currently a postdoctoral  
982 researcher at Politecnico di Torino, working in the field of  
983 high-speed optical access networks. 984
- Valter Ferrero** (M'97) received the Laurea degree (summa cum  
985 laude) in Electronics Engineering in 1994 from Politecnico di  
986 Torino, Italy. In 1994, he collaborated with Politecnico di Torino,  
987 working on coherent optical systems. From 1995 to 1996, he  
988 was with GEC Marconi, Genova, Italy. In 1997, he was in charge  
989 of the Optical Laboratory, Department of Electrical Engineering,  
990 Politecnico di Torino, and became Assistant Professor in 2001.  
991 He is currently with the Optical Communications Group,  
992 Politecnico di Torino. His current research interests include optical  
993 coherent communications, free-space optical communications, and  
994 next-generation passive optical networks. 995  
996
- Maurizio Valvo** received a M.Sc. degree in Electronics  
997 Engineering cum laude at the University of Naples (Italy) in  
998 999

1000 1991. In the same year, he joined CSELT, the Telecommunications  
1001 Research Centre and Laboratories, which is now TIM Lab–Turin  
1002 and where he is currently active. He has focused since the begin-  
1003 ning of his career on broadband access networks and, in particular,  
1004 on PON systems, which he has also contributed to specify, develop,  
1005 and test during the 1990s in the framework of several European-  
1006 funded projects. He has led research projects with the objective to  
1007 specify and test, both in the laboratory and in the field, innovative  
1008 access network technologies based on PON, xDSL, HFC, Wimax,  
1009 and free space optics. He currently leads the laboratory for fixed  
1010 access network innovation and a research project for the innova-  
1011 tion of the Telecom Italia optical access network. He holds four  
1012 patents and is the co-author of three books and several papers.

1013 **Roberto Gaudino**, Ph.D., is currently an associate professor at  
1014 Politecnico di Torino, Italy. His main research interests are in  
1015

long-haul DWDM systems, fiber nonlinearity, modeling of 1016  
optical communication systems, and in the experimental imple- 1017  
mentation of optical networks, with a specific focus on access net- 1018  
works. In particular, in the last five years, he focused his activity on 1019  
short-reach optical links using plastic optical fibers (POF) and on 1020  
next-generation passive optical access networks (NG-PON2). 1021  
Currently, he is working on ultra-high-capacity systems for 1022  
medium-reach links. Previously, he worked extensively on 1023  
fiber modeling, optical modulation formats, coherent optical 1024  
detection, and on the experimental demonstration of packet- 1025  
switched optical networks. He is the author or co-author of 1026  
more than 200 papers in the field of optical communications. 1027  
From 2009 to 2016, he was the coordinator of three projects in 1028  
the area of optical access (EU FP6-IST STREP “POF-ALL” 1029  
and “POF-PLUS” and EU FP7-ICT STREP project 1030  
“FABULOUS”). He is now the coordinator of the PhotoNext center 1031  
at POLITO. 1032

# Queries

1. AU: For Ref. [9], I have replaced the et al. with the names of the other authors based on this reference:  
<https://www.osapublishing.org/jlt/abstract.cfm?uri=jlt-34-7-1628>Please confirm that the change is correct.
2. AU: Please provide all the author names in place of “et al.” in 'Ref. [32]' as per journal style requirement.
3. AU: For Ref. [32], I have added the author names, based on this reference:<http://ieeexplore.ieee.org/document/7096918/authors?ctx=authors>Please confirm that this change is correct.